Quasiparticle band structure, exciton, and optical properties of few-layer blue phosphorus

Ju Zhou,[1] Tian-Yi Cai,[1,*] and Sheng Ju[1,2,3,†]

[1]*Department of Physics, Soochow University, Suzhou 215006, People's Republic of China*
[2]*Department of Physics, University of California at Berkeley, California 94720, USA*
[3]*Materials Sciences Division, Lawrence Berkeley National Laboratory, Berkeley, California 94720, USA*

(Received 31 August 2021; revised 18 November 2021; accepted 19 November 2021; published 3 December 2021)

The evolution of quasiparticle electronic structure, exciton, and optical properties in the few-layer blue phosphorus has been studied with the many-body perturbation method. The quasiparticle band gap decreases gradually with increasing the layer number and the system will finally evolve to metallic state in the bulk form. In spite of the increasing thickness in these indirect-band-gap semiconductors, the exciton-dominated optical properties with large binding energies are still found in the few-layer systems. With increasing layer number, the overall dielectric screening gets enhanced. However, the persistent large joint density of states associated with the parallel band structure in blue phosphorus gives rise to a much larger binding energy than the value predicted in an effective screening model. Our studies have not only provided a deep understanding of excitons in 2D semiconductors but also provided solid data for further experimental exploration of the application of few-layer blue phosphorus in optoelectronics.

DOI: 10.1103/PhysRevB.104.245401

I. INTRODUCTION

Since the discovery of black phosphorene [1–3], this new member in two-dimensional (2D) material family has attracted wide interest in condensed matter physics and material science. Black phosphorene is a narrow-band-gap semiconductor with a direct band gap (2.1 eV) and anisotropic optical properties (1.6 eV difference in the optical absorption edge between the polarization along the zigzag and armchair directions of 2D puckered structure) [4–7]. Such unique optical properties make it very useful for optoelectronic applications. For phosphorus, many allotropes have been identified in the bulk form [8] as well as the 2D form [9,10]. For the phosphorus with fibrous structure, including red phosphorus [11] and violet phosphorus [12,13], the one-dimensional tube structure with P pentagon ring will lead to enhanced excitonic effect in the optical responses. In particular, in 2D limit, Hittorf's (violet) phosphorene has been found to exhibit unusual electronic and optical properties [14]. The direct band gap (quasiparticle) of 3.32 eV, optical gap of 2.41 eV with the large exciton binding energy of 0.91 eV, and relatively short exciton lifetime (18 ns), making Hittorf's phosphorene promising for the application as green light-emitting-diodes [14].

Under high pressure, black phosphorus will undergo a structural phase transition to a layered semimetallic phase (A7 phase) [15]. In both black phosphorus and A7 phase, P atom has three nearest neighbors within the layer. However, the former exhibits an orthorhombic crystal cell with a puckered in-plane atomic arrangement while the latter has a rhombohedral cell with a buckled in-plane atomic arrangement [16]. Superconductivity has been found in the A7 phase with transition temperature around 6–13 K [17]. Recently, such kind of phase transition has also been identified in the few-layer systems [18]. The layered structure and novel transport properties of the A7 phase phosphorus have triggered many attempts towards the realization of its single-layer form, named as blue phosphorene by Zhu and Tománek [19]. In fact, by now based on the bottom-up growth technique on certain substrates [20–28], some experiments have successfully achieved the fabrication of the blue phosphorene. However, the metallic substrate is found to strongly interact with phosphorus atoms and will finally renormalize the intrinsic band structure of the 2D membrane. To reduce the interaction between phosphorene and the metallic substrate, tellurium-monolayer-supported Au(111) [22] substrate has been used to realize quasi-free-standing blue phosphorene. Later, silicon intercalation is introduced to tune the interfacial interaction of blue phosphorene with the metallic substrate [27]. Recently, a stable fabrication of blue phosphorene has also been achieved on Cu_3O_2/Cu(111) substrate [28]. However, theoretical prediction shows that blue phosphorene can be readily realized on semiconductor GaN(001) substrate with an intriguing half-layer-by-half-layer growth mechanism [29], making its further applications in optoelectronics possible.

Blue phosphorene is predicted to be an indirect-band-gap semiconductor [19]. Quasiparticle and excitonic properties of blue phosphorene have also been studied, including single-layer [30], bilayer [31] and its heterostructure with black phosphorene [32]. More recently, the unusual strain dependences of quasiparticle electronic structure, exciton, and optical properties of blue phosphorene have been revealed [33]. The funnel effect realized in the inhomogeneously strained 2D membrane could overcome the indirect-band-gap nature for the green and blue light-emitting applications [33].

*caitianyi@suda.edu.cn
†jusheng@suda.edu.cn

In a 2D system, the exciton effect is strongly enhanced due to the less screened Coulomb interaction and the optical properties of 2D materials are dominated by excitonic effect [34–47]. Electronic and optical properties will change significantly during the transition from the 2D structure to three-dimensional (3D) case. The layer dependence of quasiparticle electronic structure and optical properties have been studied in the few-layer MoS_2 [42] and black phosphorus [43–45]. Unlike the direct-band-gap semiconductors MoS_2 with parabolic band dispersion (at K and K' points) and black phosphorus with anisotropic band dispersion (at Γ point), the blue phosphorene has an indirect band gap, where the almost parallel bands for the optical transitions lead to unusual exciton formation and character [33]. With increasing the number of layers in blue phosphorene, whether the indirect-band-gap nature persists or not and what is the layer dependence of excited states are still not clear. Therefore, in this paper, based on the first-principle *GW*-BSE (Bathe-Salpeter equation) method [48], we study the quasiparticle electronic structure, exciton, and optical properties of few-layer blue phosphorus. The layer dependence is found to be different from that observed in the few-layer MoS_2 [42] and black phosphorus [43,44]. Although the overall dielectric screening increases linearly with the layer number in the few-layer systems, the large joint density of states (JDOS) accompanied with enhanced exciton mass is found to give rise to a stronger binding energy than the 2D screened model consideration. Our study provides the unique aspects of excitonic properties in the 2D materials with parallel band structure. Furthermore, the tunable optical properties could find their potential applications in 2D optoelectronics.

II. COMPUTATIONAL METHOD

The ground-state calculations of few-layer blue phosphorus are performed using density-functional theory (DFT) as implemented in QUANTUM ESPRESSO [49]. To avoid spurious interactions between layers, a vacuum layer of 16 Å along the out-of-plane direction is adopted on the simulation cell of few-layer phosphorus. We use the generalized gradient approximation of Perdew-Burke-Ernzerhof (PBE) [50] and norm-conserving pseudopotentials with a plane-wave cutoff of 60 Ry [51]. The ground-state wave functions and eigenvalues are calculated with a k grid of $30 \times 30 \times 1$ for few-layer blue phosphorus and $30 \times 30 \times 12$ for bulk phosphorus. The crystal structures are relaxed until the total forces are less than 10^{-4} eV/Å and the convergence criterion for total energies is set to 10^{-7} eV. The DFT-D2 correction is used to consider the van der Waals interaction [52].

The quasiparticle band structure and optical properties are calculated with BERKELYGW [53–55]. The quasiparticle self-energies are obtained by solving the following Dyson equation:

$$\left[-\tfrac{1}{2}\nabla^2 + V_{\text{ion}} + V_{\text{H}} + \Sigma\left(E^{\text{QP}}_{n\mathbf{k}}\right)\right]\psi^{\text{QP}}_{n\mathbf{k}} = E^{\text{QP}}_{n\mathbf{k}}\psi^{\text{QP}}_{n\mathbf{k}}, \quad (1)$$

where Σ is the self-energy operator within the *GW* approximation, and $E^{\text{QP}}_{n\mathbf{k}}$ and $\psi^{\text{QP}}_{n\mathbf{k}}$ are the quasiparticle energies and wave functions, respectively. Generalized plasmon pole model is used in the calculation. A truncated Coulomb interaction between the blue phosphorus and its periodic image is adopted. To ensure the convergence of quasiparticle energies [56], we use a coarse k grid of $30 \times 30 \times 1$, empty bands of 100 times more than the valence bands, and the dielectric cutoff of 10 Ry for few-layer blue phosphorus [33].

The static polarizability is firstly calculated from random-phase approximation from

$$\chi_{\mathbf{GG}'}(\mathbf{q};0) = \sum_{n,n',\mathbf{k}} \langle n,\mathbf{k}|e^{-i(\mathbf{q}+\mathbf{G})\cdot\mathbf{r}}|n',\mathbf{k}+\mathbf{q}\rangle\langle n',\mathbf{k}+\mathbf{q}| \times e^{i(\mathbf{q}+\mathbf{G}')\cdot\mathbf{r}'}|n,\mathbf{k}\rangle \frac{1}{E_{n'\mathbf{k}+\mathbf{q}} - E_{n\mathbf{k}}}, \quad (2)$$

where n and n' are occupied and unoccupied band indices, $\mathbf{k}$ is wave vector, $\mathbf{q}$ is a vector in the first Brillouin zone, $\mathbf{G}$ is a reciprocal-lattice vector, and $|n,\mathbf{k}\rangle$ and $E_{n\mathbf{k}}$ are the mean-field electronic eigenvectors and eigenvalues. Then the dielectric matrix is constructed as

$$\epsilon_{\mathbf{GG}'}(\mathbf{q};0) = \delta_{\mathbf{GG}'} - v(\mathbf{q}+\mathbf{G})\chi_{\mathbf{GG}'}(\mathbf{q};0), \quad (3)$$

where $v(\mathbf{q}+\mathbf{G}) = 4\pi/|\mathbf{q}+\mathbf{G}|^2$ is the bare Coulomb interaction.

The electron-hole excitations are then calculated by solving the BSE equation for each exciton state S:

$$\left(E^{\text{QP}}_{c\mathbf{k}} - E^{\text{QP}}_{v\mathbf{k}}\right)A^S_{vc\mathbf{k}} + \sum_{v'c'\mathbf{k}'}\langle vc\mathbf{k}|K^{\text{eh}}|v'c'\mathbf{k}'\rangle A^S_{v'c'\mathbf{k}'} = \Omega^S A^S_{vc\mathbf{k}}, \quad (4)$$

where $A^S_{vc\mathbf{k}}$ is the exciton wave function, Ω^S is the excitation energy, and K^{eh} is the electron-hole interaction kernel. Finally, we obtain the imaginary parts of frequency-dependent complex dielectric function $\epsilon_2(\omega)$ as

$$\epsilon_2(\omega) = \frac{16\pi^2 e^2}{\omega^2}\sum_S |\mathbf{e}\cdot\langle 0|\mathbf{v}|S\rangle|^2\delta(\omega-\Omega^S), \quad (5)$$

where $\mathbf{v}$ is the velocity operator and $\mathbf{e}$ is the polarization of the incoming light. A Gaussian smearing with a broadening constant of 20 meV is used in optical absorption spectrum. For the convergence of BSE calculations, a fine k grid of $120 \times 120 \times 1$ is used. It is noted that fine sampling is necessary to capture fast variation in screening at small wave vectors and fine features in exciton wave functions, which are tightly localized in k space.

The absorbance A of few-layer blue phosphorus is expressed as

$$A(\omega) = 1 - e^{-\alpha(\omega)d} = 1 - e^{-\frac{\omega\epsilon_2 d}{\hbar c}}, \quad (6)$$

where α is the absorption coefficient, d is the thickness of the simulation cell along the direction perpendicular to the layer, ϵ_2 is the imaginary part of the dielectric function, and ω is the photon energy.

Using Fermi's golden rule, the radiative lifetime $\tau_S(0)$ at 0 K of an exciton in state S is derived according to [57,58]

$$\tau_S(0) = \frac{\hbar^2 c}{8\pi e^2 E_S(0)}\frac{A_{\text{uc}}}{\mu_S^2}, \quad (7)$$

where c is the speed of light, A_{uc} is the area of the unit cell, $E_S(0)$ is the energy of the exciton in state S, and $\mu_S^2 = (\hbar^2/m^2E_S(0)^2)(|\langle G|p_{||}|\Psi_S\rangle|^2/N_k)$ is the square modulus of the BSE exciton transition dipole divided by the number of unit cells in this 2D system. The exciton radiative lifetime $\langle\tau_S\rangle$ at

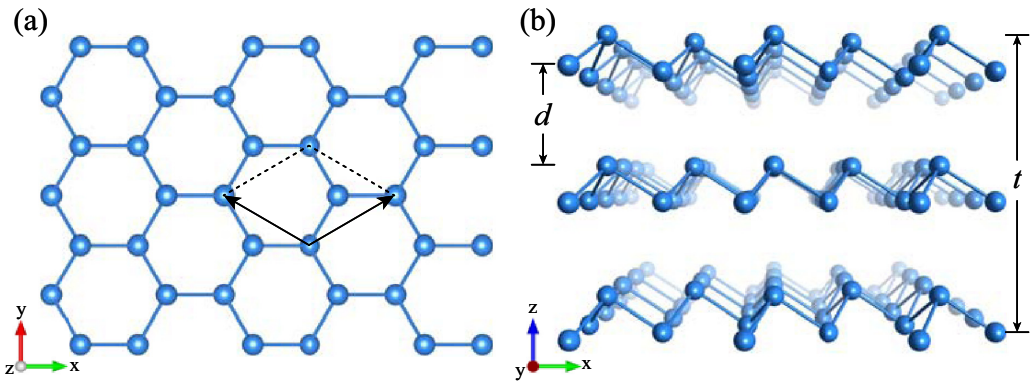

FIG. 1. Crystal structure of trilayer blue phosphorus with AA stacking. (a) Top view. (b) Side view.

temperature T is obtained as [58]

$$\langle \tau_S \rangle = \tau_S(0)\frac{3}{4}\left(\frac{E_S(0)^2}{2M_S c^2}\right)^{-1} k_B T, \tag{8}$$

where k_B is the Boltzmann constant, and $M_S = m_e^* + m_h^*$ is the exciton effective mass as the exciton energy dispersion $E_S(Q) = E_S(0) + \hbar^2 Q^2/2M_S$ is employed with Q being the center-of-mass momentum of the exciton.

III. RESULTS AND DISCUSSION

While sharing the atomic connectivity with the honeycomb lattice of graphene, the crystal structure of each layer in blue phosphorus is nonplanar. The theoretically optimized lattice constant for monolayer blue phosphorene is 3.28 Å with a P-P bond of 2.26 Å and an effective thickness t is 1.24 Å [33]. To mimic the epitaxial growth of possible few-layer and even multilayer blue phosphorus, the in-plane lattice constant is fixed to 3.28 Å of the monolayer. For the bilayer blue phosphorus, we find that AA stacking is the most energetically favorable (see Appendix A). Therefore, we focus on AA stacking to discuss the evolution of quasiparticle band structure, exciton, and optical properties in few-layer blue phosphorus. As shown in Fig. 1, the optimized crystal structure for trilayer blue phosphorus has an effective thickness of 10.18 Å and interlayer distance of 3.23 Å. As the number of layers increases, the effective thickness increases but the interlayer distance changes little. For pentalayer system, t is 19.12 Å. Detailed parameters of effective thickness and interlayer distance are listed in Table I. Our considerations are also consistent with previous theoretical results, where for the bilayer structure as well as few-layer systems of blue phosphorus, AA stacking was found to be energetically favorable and the system was mechanically and thermodynamically stable [31,59,60]. It is noted that the pressure-driven A7 phase has A′B stacking ordering [15–18], which in the fully optimized condition the bilayer crystal structure has a much closer interlayer distance of 1.82 Å as well as shorter interlayer P-P bonding of 2.67 Å. In contrast to semiconducting nature in all the other stackings, the metallic state is coherent to this non-van der Waals crystal structure [61].

TABLE I. Effective thickness and interlayer distance of few-layer blue phosphorus.

	monolayer	bilayer	trilayer	quadlayer	pentalayer
t (Å)	1.24	5.84	10.18	14.64	19.12
d (Å)	—	3.36	3.23	3.23	3.23

The quasiparticle (G_0W_0) band structures of few-layer blue phosphorus are presented in Fig. 2. The PBE results are also presented. All the few-layer systems exhibit indirect-band-gap nature, and the band gap decreases with increasing the number of layers, i.e., from 3.41 eV for monolayer to 1.09 eV for pentalayer. The blue phosphorus finally becomes metallic in the bulk form (see Appendix B). The valence band maximum (VBM) is firstly located at Γ point in monolayer and changes to the point near Γ point in few-layer phosphorus. The conduction band minimum (CBM) is almost unchanged for monolayer up to quadlayer, locating along the Γ-M line. For pentalayer blue phosphorus, it changes to K point. Compared to G_0W_0 results, PBE bands show much reduced band gap. The band dispersion, however, changes little.

The evolution of quasiparticle (G_0W_0) indirect band gap with the number of layers N is presented in Fig. 3. Since the bulk blue phosphorus is metallic (semimetal), we fit the data of the band gap up to five layers to achieve the power law. The quasiparticle gaps are found to obey a power law of the form $(A/N^x + B)$, with the fitting parameters of $E_g = 11.52/N^{0.14} - 8.09$. A similar trend is also found in PBE results, with $x = 0.15$, $A = 8.76$, and $B = -6.83$. Within this kind of approach, we find that the decay of the band gap in few-layer blue phosphorus is obviously faster than $1.70/N^{0.73} + 0.30$ law revealed in few-layer black phosphorus and $2.09/N^{0.61} + 0.65$ law revealed in few-layer MoS_2, where the bulk of these two materials are semiconductors [42,43].

The direct transition energy for the lowest interband transitions in few-layer blue phosphorus is presented in Fig. 4. All the few-layer blue phosphorus are found to exhibit similar character of transitions with six deep valleys in the first Brillouin zone. As the number of layers increases, the depth at the center of valley decreases, from 3.69 eV in monolayer to 2.36 eV in pentalayer. Besides, the dispersion of the direct transition energy becomes flatter in thicker structures. Such kind of energy profile should be very important for optical transitions in blue phosphorene [33].

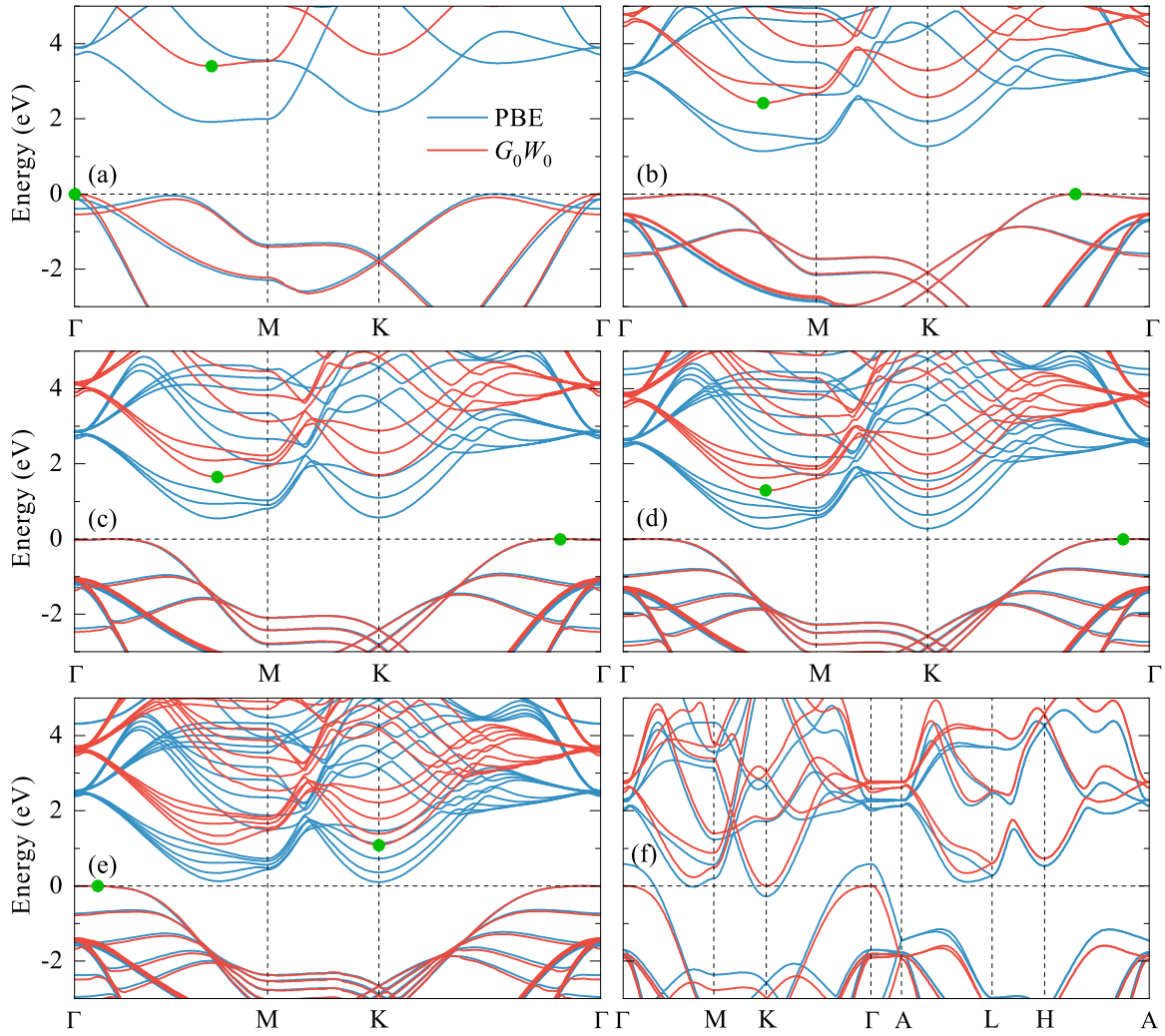

FIG. 2. Quasiparticle (G_0W_0) band structure (in contrast to PBE bands) of few-layer blue phosphorus. The dots indicate VBM or CBM. (a) monolayer, (b) bilayer, (c) trilayer, (d) quadlayer, (e) pentalayer, and (f) bulk.

With the above revealed band profile, the optical absorption spectrum of few-layer blue phosphorus is presented in Fig. 5. It is necessary to consider electron-hole interaction to describe the exciton-dominated optical absorption peaks in the few-layer blue phosphorus. Strong exciton effect is obvious in all the systems. With increasing layer number, the exciton binding energy in the few-layer blue phosphorus decreases from 0.84 eV in monolayer to 0.33 eV in pentalayer. The value is still much larger than that in conventional 3D semiconductors. The absorption peaks also become lowered and get being continuous in thicker systems. The absorption edge decreases from 2.85 eV in monolayer to 2.04 eV in pentalayer, showing the incorporation of a much wide range of visible light spectrum for 2D photovoltaics.

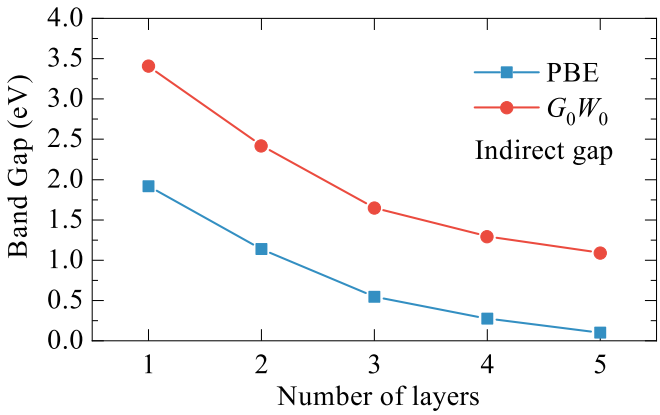

FIG. 3. Layer dependence of quasiparticle indirect band gaps in few-layer blue phosphorus. PBE results are also shown for the comparison.

Similar to monolayer blue phosphorene, the optical transitions for the first absorption peak in the few-layers happens around Λ point [33]. The evolution of quasiparticle and optical band gap with the number of layers for the optical transition (at Λ point) is presented in Fig. 6. Λ point is defined as the center of the transition of the first bright exciton, which will also be explained in detail in the following. The dependence is found to obey the power law in the form $2.11/N^{0.64} + 1.59$ and $1.34/N^{0.63} + 1.52$ for quasiparticle and optical band gap, respectively. It is noted that for few-layer black phosphorus, the optical band gap obeys $0.87/N^{0.96} + 0.28$ [43]. Such kind

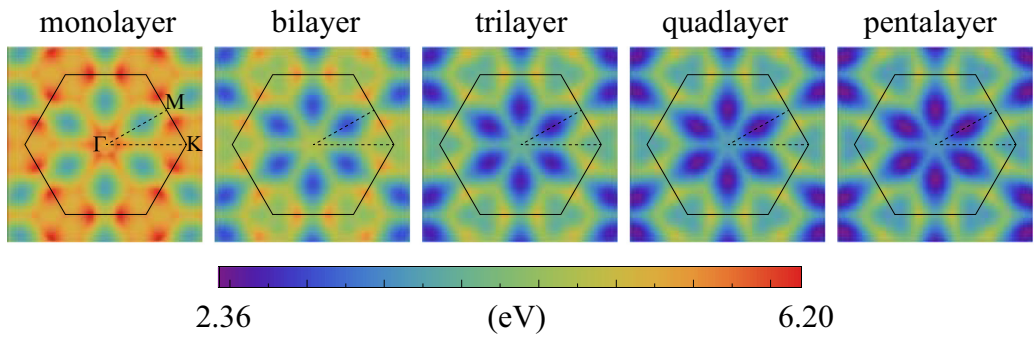

FIG. 4. Layer dependence of direct band gap (the lowest interband transitions) in few-layer blue phosphorus.

of difference is attributed to the band dispersion characters near the optical transition, i.e., anisotropic dispersion near Γ in black phosphorene, parabolic dispersion near K(K′) in MoS_2, and almost parallel bands dispersion near Λ in blue phosphorene. For few-layer blue phosphorus, such unique character persists.

The exciton energy spectrum of few-layer blue phosphorus is presented in Fig. 7. Here, we regard the exciton with the oscillation strength higher than 10^{-5} as the bright exciton, otherwise, regard as dark state. Similar to other 2D materials, the nonuniform screening leads to such non-Rydberg series of exciton states [33,41].

To understand the exciton formation associated with the optical transition in few-layer phosphorus, we plot the envelope function times oscillation strength of the first bright exciton as shown in Fig. 8. The amplitude decreases dramatically as increasing the number of layers, consistent with the decreased absorption amplitude revealed above. Besides, the transitions are highly localized in six valleys, with distribution area becoming smaller in thicker structure, indicating weaker exciton effect for the combination of electron-hole pairs in thicker structure. The detailed distribution along 1D path (from Γ to M) for exciton formation is presented in Fig. 9. We find the exciton is mostly contributed by the transition from the highest valence band (v1) and the lowest conduction band (c1). The center of the exciton, i.e., Λ point, corresponds to the lowest transition energy and largest transition matrix element, with the blue arrows with decreasing strength of the half-height width in the envelope function. With increasing the layer number, the center shifts left hand side, getting much closer to Γ point. It is noted that few-layer blue

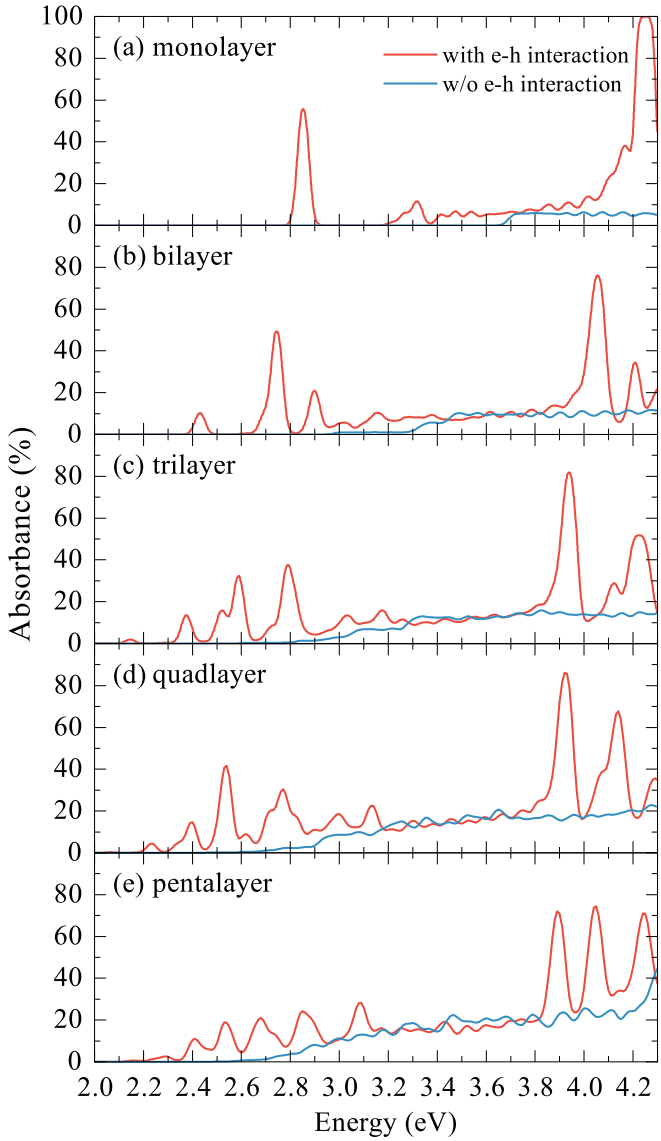

FIG. 5. Layer dependence of optical absorption in few-layer blue phosphorus. Results without considering the electron-hole interactions are also shown for the comparison.

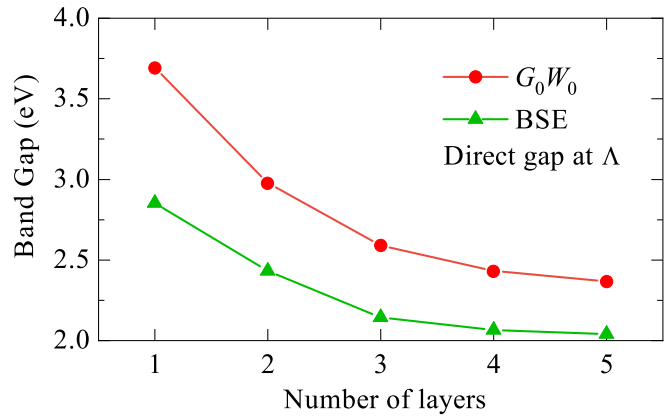

FIG. 6. Layer dependence of optical band gap (BSE) and the quasiparticle band gap (G_0W_0) at Λ point.

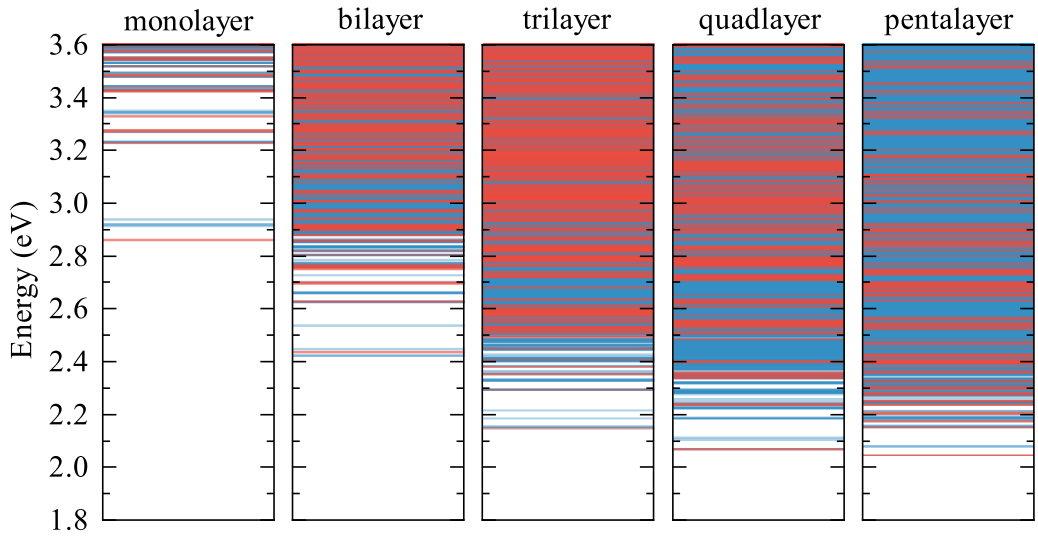

FIG. 7. Exciton energies in few-layer blue phosphorus. Red and blue lines are for bright and dark excitons, respectively.

phosphorus are indirect band gap semiconductors. Using monolayer blue phosphorene as an example, we try to evaluate the contribution from indirect transitions in this indirect band gap semiconductor (see Appendix C). It is found that the transition from Γ point to CBM is comparable to that of the direct transition at Λ point. Meanwhile, the transition energy from Γ to CBM is 0.28 eV lower than that of the direct transition at Λ point. Therefore, when considering the temperature effect [62,63], excitons with lower energies could form and optical absorption spectrum of few-layer blue phosphorus will exhibit a red-shift.

To understand the exciton in few-layer systems further, we plot the real-space distribution of modulus squared wave function of the first bright exciton. The monolayer of blue phosphorene is presented in Fig. 10. Here, we fix the hole at the center of the P-P bond. The radially symmetric distribution is consistent with the 1*s* exciton envelope function in reciprocal space. As seen from the side view in Fig. 10(b), the exciton distribution is limited within the layer due to the quantum confinement effect. Similar to the monolayer, the first bright exciton in the bilayer blue phosphorus also shows 1*s* like symmetric distribution [see Fig. 11(a)]. However, due to the bilayer structure, as indicated in Fig. 11(b), the exciton wave function as well as its planar average show equal distribution between two layers, indicating the mixing of both intralayer and interlayer excitonic characters. Similarly, the real-space plots of the first bright exciton in trilayer, quadlayer, and pentalayer, as presented in Figs. 12, 13, and 14, respectively, exhibit interlayer characteristics. The position of the hole is adjusted to investigate the distribution of electrons. It is noted that the planar distribution radius increases with the number of layers and the electron-hole excitation gets more accumulated in the inner layers. The quantum confined surface layer has smaller electron-hole excitation for the first excitonic state, but the mixing of interlayer characteristics is evident. It is also noted that as the number of layers increases, the proportion of intralayer exciton gets decreased, which also agrees with the weaker exciton oscillation strength (Fig. 8) and absorption strength (Fig. 5) in thicker blue phosphorus.

By now, we could summarize the evolution of the excitonic properties in the few-layer blue phosphorus. The *N* dependencies of exciton effective mass, exciton binding energy, and exciton lifetime for the first bright exciton are presented in Fig. 15. As shown in Fig. 15(a), the exciton effective mass increases when the number of layers is increased. Effective masses of the electron and hole show a similar trend (see the inset). The exciton binding energy, however, decreases with increasing number of layers [see Fig. 15(b)]. The dielectric

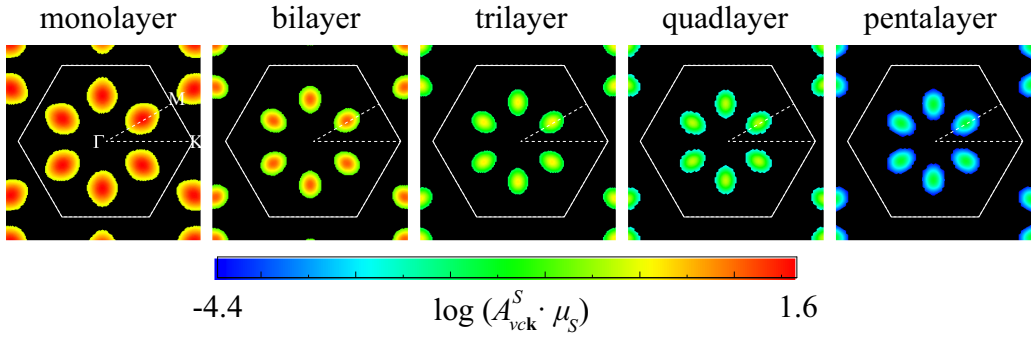

FIG. 8. Reciprocal plots for the strength of the first bright exciton. The decrease of exciton magnitude with increasing layer number is evident.

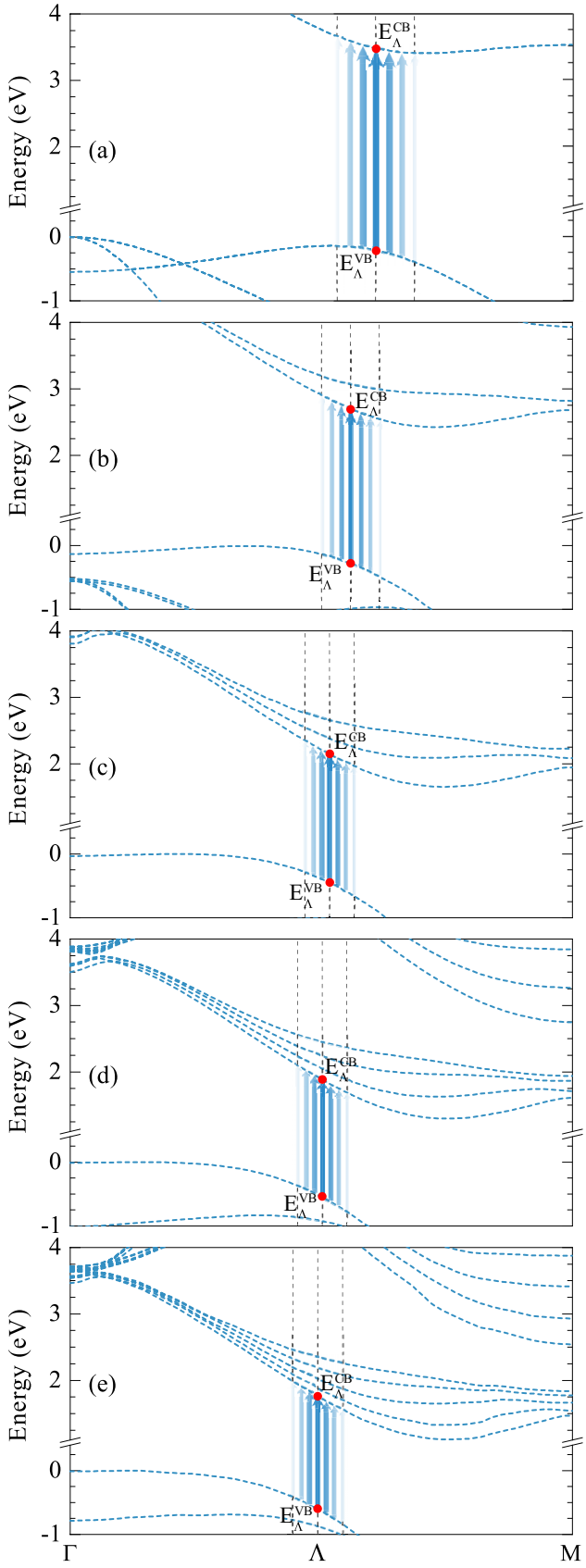

FIG. 9. Quasiparticle band structure with the distribution of optical transitions composing the first bright excitonic state in few-layer blue phosphorus: (a) monolayer, (b) bilayer, (c) trilayer, (d) quadlayer, and (e) pentalayer.

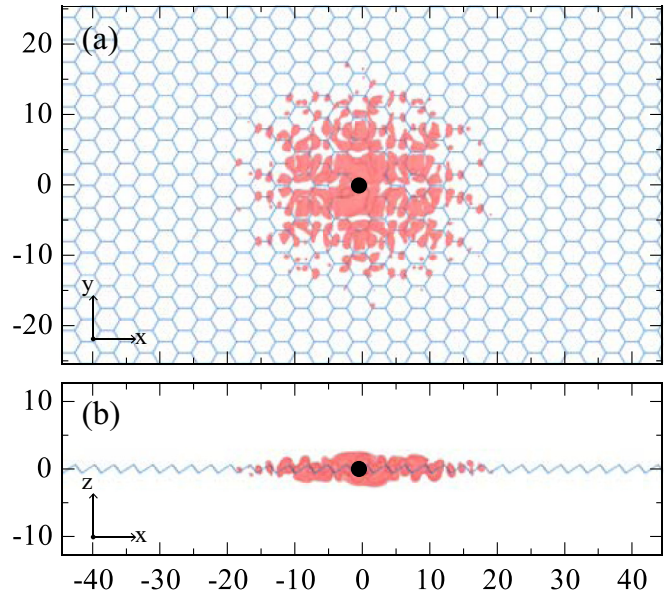

FIG. 10. Real-space plots of modulus squared of the first bright exciton wave function in monolayer blue phosphorene. Here, the hole (black circle) is fixed at the center of the bond between two neighboring phosphorus atoms.

screening becomes stronger in thicker layers and weakens the electron-hole interaction. As shown in Fig. 15(c), the exciton lifetime at room temperature (300 K) increases significantly with increasing number of layers. The main reason for such dramatic increase is the rapid decrease of the oscillation strength. The exciton lifetime increases from 0.24 ns for the monolayer to 3.39×10^3 ns for the pentalayer. Such a wide tunability should be beneficial for the applications of optoelectronic devices.

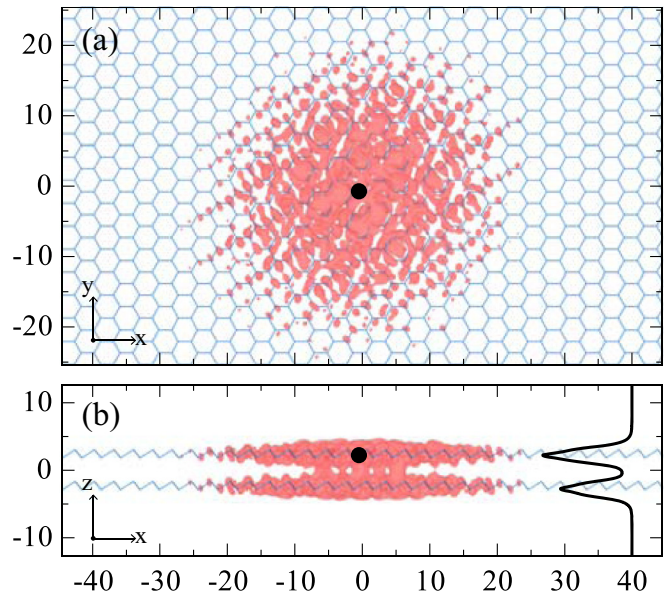

FIG. 11. Real-space plots of modulus squared of the first bright exciton wave function in bilayer blue phosphorus. Here, the hole (black circle) is fixed at the center of the bond between two neighboring phosphorus atoms.

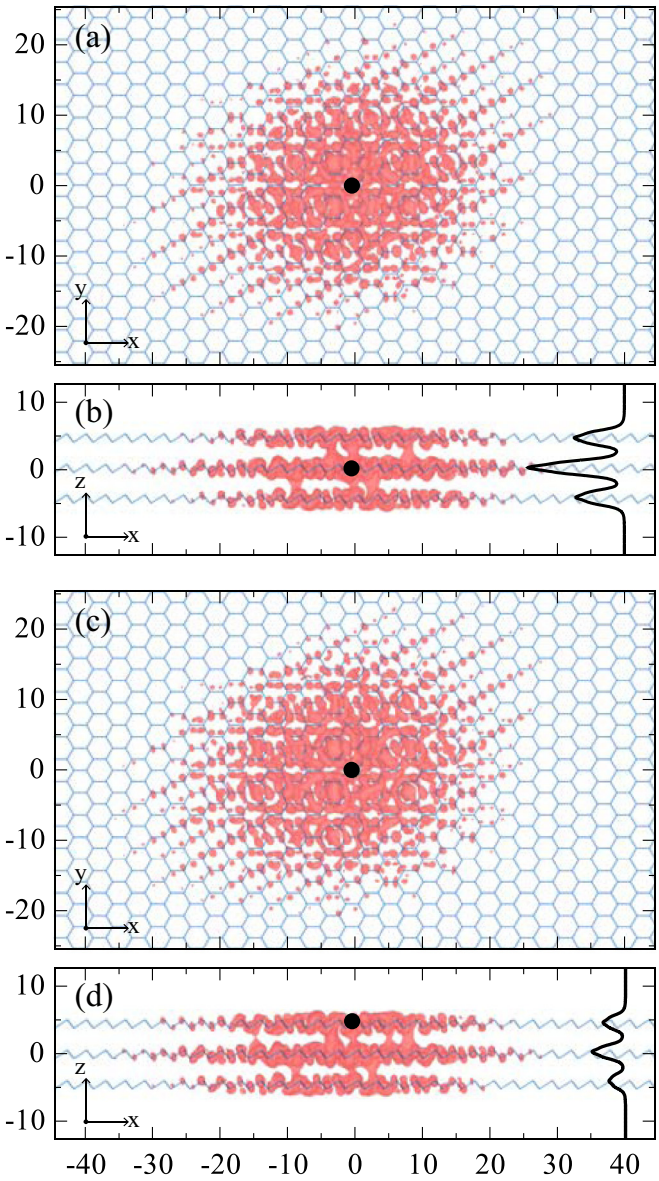

FIG. 12. Real-space plots of modulus squared of the first bright exciton wave function in trilayer blue phosphorus. Here, the hole (black circle) is fixed at the center of the bond between two neighboring phosphorus atoms.

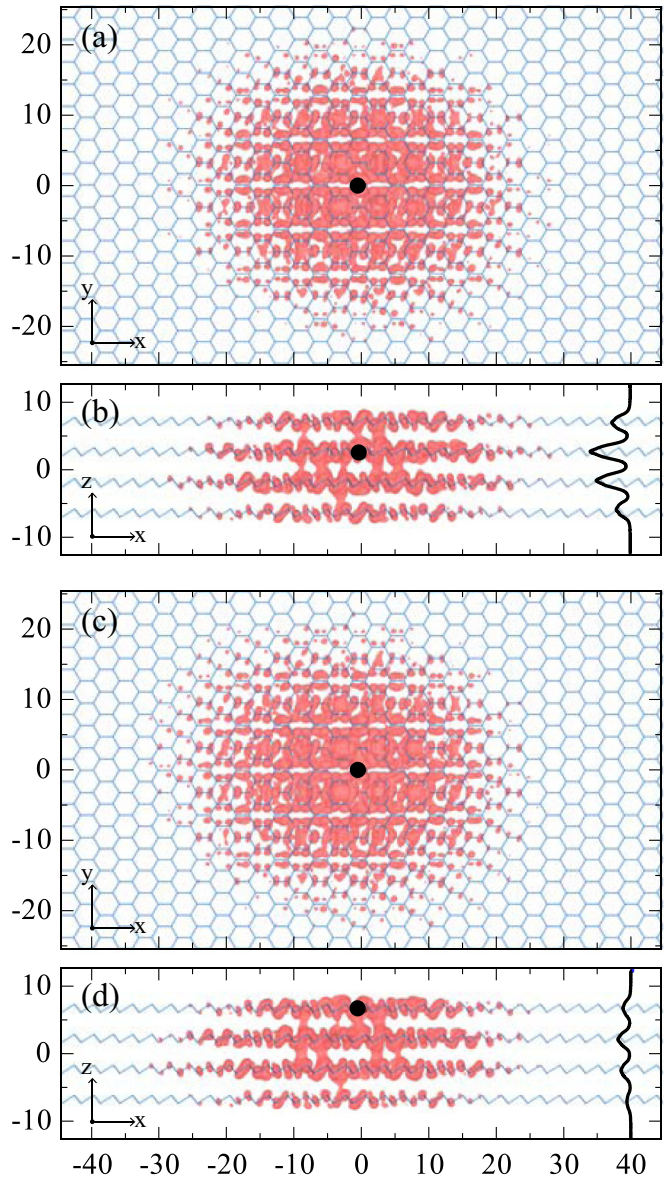

FIG. 13. Real-space plots of modulus squared of the first bright exciton wave function in quadlayer blue phosphorus. Here, the hole (black circle) is fixed at the center of the bond between two neighboring phosphorus atoms.

The above dependencies in fact agree with the evolution of dielectric screening in 2D materials, which is nonuniform with the q dependence of dielectric function presented in Fig. 16(a) for few-layer blue phosphorus. Similar to other 2D materials, the inverse dielectric function starts from the unity (ϵ_0 in the vacuum) for the long-wavelength limit, then decreases to the minimum and finally increasing toward the unity [41]. Clearly, since the increasing of the number of layers naturally enhances the dielectric screening of Coulomb interaction, the inverse dielectric function becomes lower in thicker few-layer blue phosphorus. Generally, the dielectric function is defined in the form $\epsilon_{2D}(q) = 1 + 2\pi\alpha_0^{2D}q$, where α_0^{2D} is the 2D polarizability [41]. The effective 2D polarizability of few-layer phosphorus is then fitted and provided in Fig. 16(b). We find that α increases linearly with the number of layers, verifying the fact that the thicker the few-layer blue phosphorus is, the stronger the dielectric screening will be.

Comparing the evolution shown in Figs. 6 and 15, we find that the exciton effective mass increases while the band gap and exciton binding energy decrease with increasing layers of blue phosphorus. In general, it is believed that in 2D systems, the larger the band gap, the stronger the exciton binding energy [64–66]. In the meantime, it is widely accepted that in semiconductors the larger the band gap, the larger the effective mass [67]. Here, the increase of the exciton effective mass is associated with the parallel band structure of few-layer blue phosphorus. The electron and the hole effective masses that compose exciton mass, are calculated at Λ point where the electron-hole pairs for the first bright exciton are located. When increasing the layer number, Λ point moves

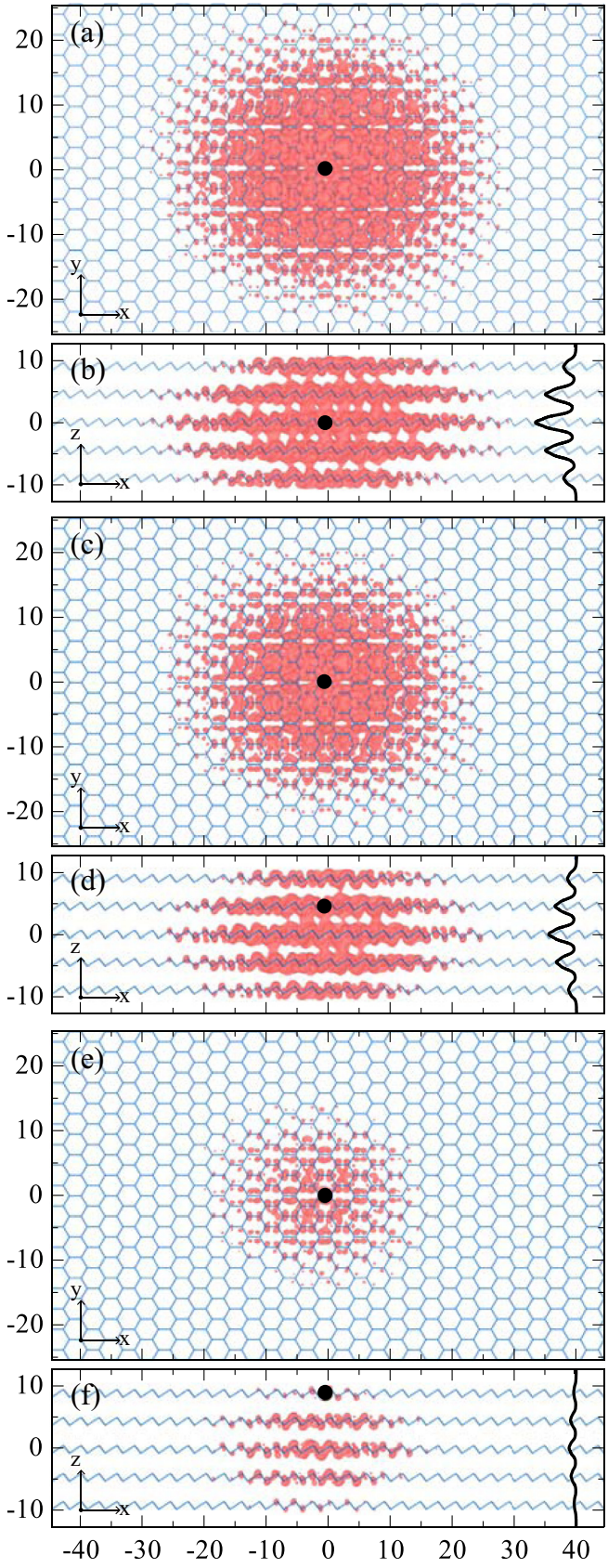

FIG. 14. Real-space plots of modulus squared of the first bright exciton wave function in pentalayer blue phosphorus. Here, the hole (black circle) is fixed at the center of the bond between two neighboring phosphorus atoms.

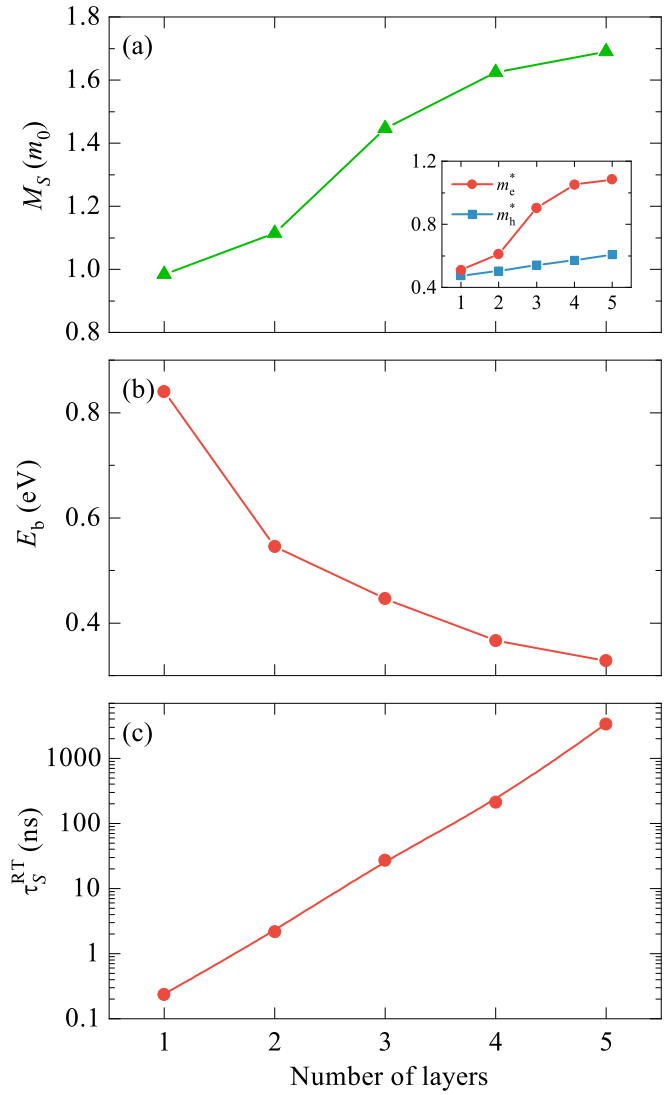

FIG. 15. Layer dependence of (a) exciton effective mass (inset is for the masses of electron and hole), (b) exciton binding energy, and (c) exciton lifetime.

farther from the local band extrema, as shown in Fig. 9, and it becomes important to incorporate nonparabolic effect in the effective mass [68]. We find that due to the nonparabolic effect, the farther Λ point locates from local band extrema, the stronger band flattening is, which results in the increase of the effective mass of the electron and the hole, and subsequently the exciton. It is interesting to proceed a little further by invoking quantitative model analysis. In a 2D system, the exciton binding energy is suggested to be proportional to m_S/ϵ^2, where $m_S = 1/(1/m_e^* + 1/m_h^*)$ is the exciton reduced mass and ϵ is the dielectric constant [64]. Typically, in 2D system with infinitesimal thickness, the dielectric constant is same as the vacuum dielectric constant, making $\epsilon = 1$ and $E_b \propto m_S$. As the number of layers increases, the dielectric screening becomes stronger and ϵ becomes essential. In a simplified screened hydrogen model [65],

$$E_b = 2m_S/\epsilon_{\text{eff}}^2, \tag{9}$$

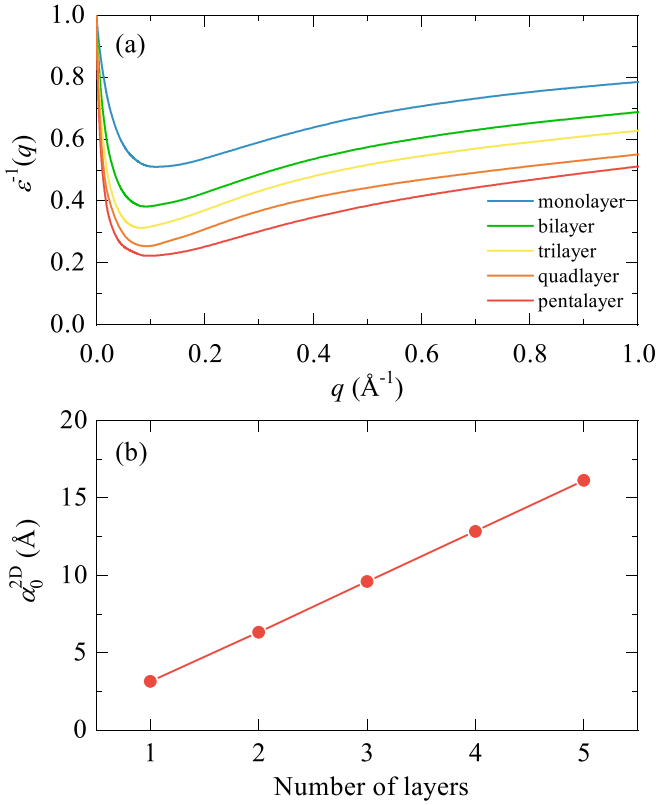

FIG. 16. (a) **q** dependence of dielectric function. (b) Layer dependence of effective screening.

where $\epsilon_{\text{eff}} = (1 + \sqrt{1 + 32\pi\alpha_0^{2D} m_S/3})/2$ is the effective dielectric constant. In Fig. 17, we scale the exciton binding energy with quasiparticle band gap for both first-principle and model calculations. A similar dependence is found between each other. However, the real magnitude of exciton is underestimated even if we have considered the first-principle dielectric screening and effective mass of exciton. In few-layer blue phosphorus, the exciton binding energy is much larger than the model predictions. The reason is due to the particular band structure as shown explicitly in Fig. 9, where the almost parallel band structure leads to strong JDOS. This is similar to bulk Si, where unlike direct-band-gap semiconductor GaAs, the parallel band structure leads to large JDOS and strong optical absorption [67]. The JDOS is defined as $J(\omega) = \sum_{vc\mathbf{k}} \delta[E_c(\mathbf{k}) - E_v(\mathbf{k}) - \hbar\omega]$. If we do not consider exciton effect (only within independent particle approximation), then the JDOS is continuous above the absorption edge. When considering the exciton effect, we define a quantity I_S to introduce the JDOS contribution to an exciton state S as $I_S = \int_S J(\omega) d\omega$, where the integral range over the transition corresponding to the half-height width of the exciton. For few-layer blue phosphorus the degeneracy of the low-energy conduction bands (c1, c2,...) near Λ point are partially removed, and the transitions from v1 to these conduction bands will compose many exciton states. For example, for the first bright exciton state as we illustrated in the bilayer system, the corresponding transitions for this exciton state are mainly from v1 to c1. There are also other exciton states based on the transitions from v1 to c2. Therefore, I_S is independent of layer number. In the following, we consider the first bright exciton which only arise from the transition of v1 to c1. As demonstrated in Fig. 18, the JDOS(interband) contribution for the first bright exciton in blue phosphorene is much larger than other 2D systems (MoS_2 and black phosphorene as calculated in Appendix D) and the magnitude persists strongly in the few-layer systems. This finding provides solid evidence that the parallel band structure could give rise to strong exciton effect in 2D materials.

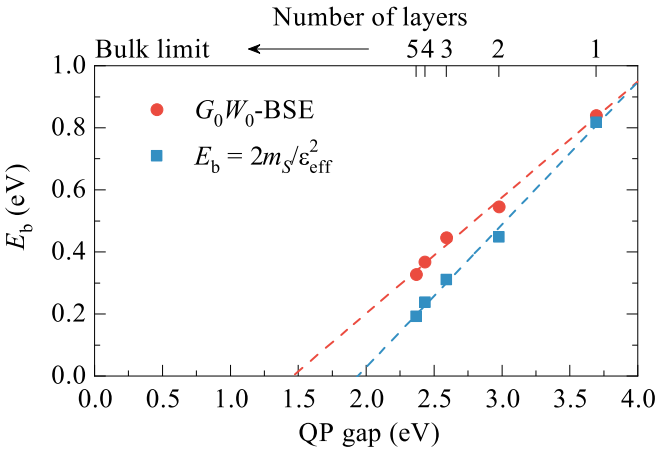

FIG. 17. The exciton binding energy versus the QP band gap for few-layer blue phosphorus. The dashed line represents the linear relation in the form of $E_b = 0.37 \times E_{\text{gap}} - 0.55$ for G_0W_0 and $E_b = 0.46 \times E_{\text{gap}} - 0.89$ for the 2D screened hydrogen model.

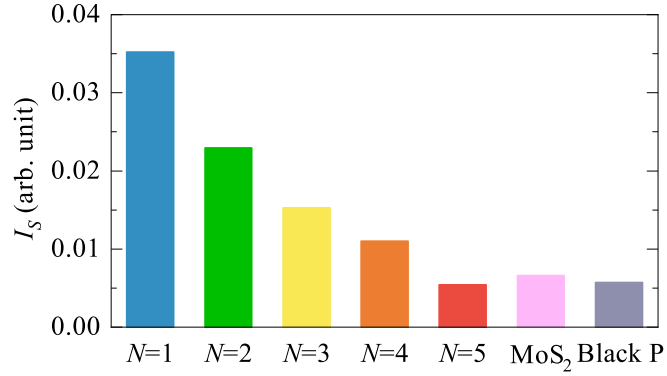

FIG. 18. I_S for the first bright exciton state in the few-layer blue phosphorus and other two 2D materials MoS_2 and black phosphorene.

IV. SUMMARY

To summarize, we have studied the quasiparticle electronic structure, exciton, and optical properties of few-layer

TABLE II. The energy difference in bilayer phosphorene with AA, AB, AB′, and AA′ stackings.

	AA	AB	AB′	AA′
ΔE (meV)	0.00	0.35	11.80	12.33

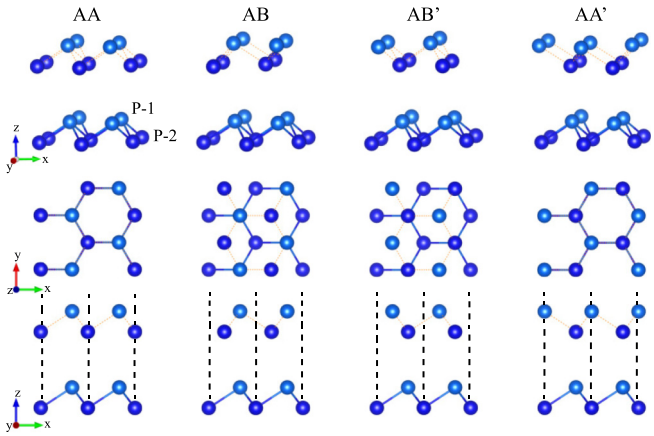

FIG. 19. Stacking ordering in the bilayer of blue phosphorus.

blue phosphorus. The unusual dielectric screening from the quantum confined geometry is well captured by the advanced many-body perturbation method (G_0W_0-BSE). The indirect band gap of 3.41 eV in the monolayer blue phosphorene gradually decreases in the few-layer systems and evolves to 1.09 eV in pentalayer. The optical absorption also shows a monotonic decrease, with the absorption edge changing from 2.85 eV in monolayer to 2.04 eV in pentalayer. The reduced band gap is accompanied with reduced exciton binding energy, consistent with the enhanced dielectric screening when the layer number is increased. However, the large JDOS accompanied with large exciton mass makes the electron-hole pairs more strongly bounded than the prediction in an effective screening model. These findings suggest the emergence of unusual excitonic effect in 2D materials with the parallel band structure. Furthermore, the tunable band gap and optical properties revealed in few-layer blue phosphorus make them an ideal platform for further experimental studies of the optoelectronic properties and applications.

ACKNOWLEDGMENTS

S.J. thanks Prof. Steven G. Louie and all his group members for their great help on BERKELEYGW method and useful discussion on exciton physics in 2D materials. This work is supported by the National Basic Research Program of China (973 Program 2019YFA0308402) and the National Natural Science Foundation of China under Grant No. 51972217.

APPENDIX A: STACKING ORDERING OF BLUE PHOSPHORUS

In Table II, we show the energies of bilayer blue phosphorus with different stacking ordering, with the crystal structures demonstrated in Fig. 19.

APPENDIX B: BULK BLUE PHOSPHORUS FROM *GW*

We use a coarse k grid of $18 \times 18 \times 6$, a fine k grid of $48 \times 48 \times 16$, empty bands of 60 times more than the valence bands (600 bands), and the dielectric cutoff of 10 Ry for the calculation. Within the G_0W_0 approach, the bulk blue phosphorus is a semimetal with a 3 meV overlap between the top of valance band and the bottom of conduction band.

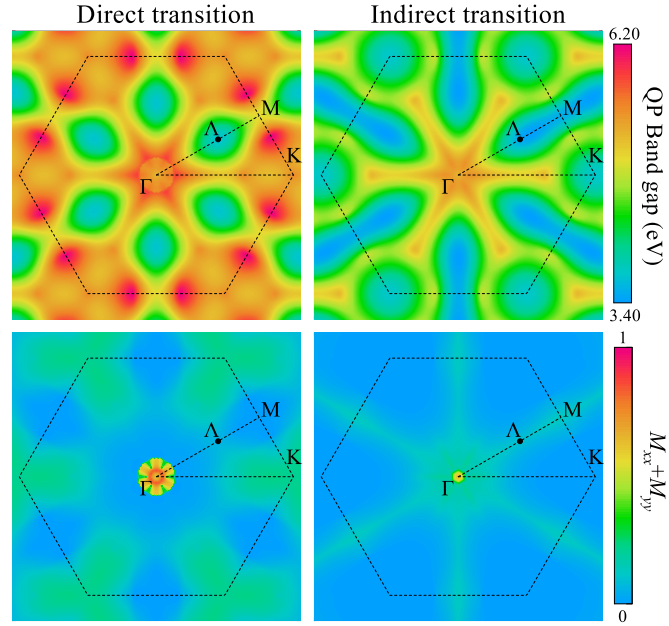

FIG. 20. Comparison between the direct (from v1 to c1) and the indirect (from Γ point at v1 to c1) transitions in monolayer blue phosphorene. The upper panels are the quasiparticle interband transition energy and the lower panels are the transition matrix.

APPENDIX C: DIRECT VERSUS INDIRECT TRANSITIONS

In Fig. 20, we calculate the direct (from v1 to c1) and the indirect (from Γ point at v1 to c1) transitions in monolayer blue phosphorene. The transition matrix from Γ point to CBM is comparable to that of the direct transition at Λ point. Meanwhile, the transition energy from Γ to CBM is lower than that of the direct transition at Λ point.

APPENDIX D: BLACK PHOSPHORENE AND MoS_2 FROM *GW*-BSE

The calculations are based on QUANTUM ESPRESSO [49] and BERKELEYGW [55] packages. The norm-conserving PBE pseudopotentials with a plane wave cutoff of 80 Ry are used. For MoS_2, we use a coarse k grid of $24 \times 24 \times 1$, empty bands of 30 times more than the valence bands, and the dielectric cutoff of 10 Ry in G_0W_0 part, and a fine k grid of $96 \times 96 \times 1$ in the BSE part. For black phosphorene, we use a coarse k grid of $18 \times 12 \times 1$, empty bands of 50 times more than the valence bands, and the dielectric cutoff of 10 Ry in G_0W_0 part, and a fine k grid of $72 \times 48 \times 1$ in the BSE part. It is noted that blue phosphorene has a stronger exciton binding energy than MoS_2 and black phosphorene [33,37,43].

[1] F. Xia, H. Wang, and Y. Jia, Rediscovering black phosphorus as an anisotropic layered material for optoelectronics and electronics, Nat. Commun. **5**, 4458 (2014).

[2] L. Li, Y. Yu, G. J. Ye, Q. Ge, X. Ou, H. Wu, D. Feng, X. H. Chen, and Y. Zhang, Black phosphorus field-effect transistors, Nat. Nanotechnol. **9**, 372 (2014).

[3] H. Liu, A. T. Neal, Z. Zhu, Z. Luo, X. Xu, D. Tománek, and P. D. Ye, Phosphorene: An unexplored 2D semiconductor with a high hole mobility, ACS Nano **8**, 4033 (2014).

[4] R. Schuster, J. Trinckauf, C. Habenicht, M. Knupfer, and B. Büchner, Anisotropic Particle-Hole Excitations in Black Phosphorus, Phys. Rev. Lett. **115**, 026404 (2015).

[5] X. Wang, A. M. Jones, K. L. Seyler, V. Tran, Y. Jia, H. Zhao, H. Wang, L. Yang, X. Xu, and F. Xia, Highly anisotropic and robust excitons in monolayer black phosphorus, Nat. Nanotechnol. **10**, 517 (2015).

[6] H. Yuan, X. Liu, F. Afshinmanesh, W. Li, G. Xu, J. Sun, B. Lian, A. G. Curto, G. Ye, Y. Hikita, Z. Shen, S. C. Zhang, X. Chen, M. Brongersma, H. Y. Hwang, and Y. Cui, Polarization-sensitive broadband photodetector using a black phosphorus vertical *p-n* junction, Nat. Nanotechnol. **10**, 707 (2015).

[7] L. Li, J. Kim, C. Jin, G. J. Ye, D. Y. Qiu, F. H. da Jornada, Z. Shi, L. Chen, Z. Zhang, F. Yang, K. Watanabe, T. Taniguchi, W. Ren, S. G. Louie, X. H. Chen, Y. Zhang, and F. Wang, Direct observation of the layer-dependent electronic structure in phosphorene, Nat. Nanotechnol. **12**, 21 (2017).

[8] F. Bachhuber, J. von Appen, R. Dronskowski, P. Schmidt, T. Nilges, A. Pfitzner, and R. Weihrich, The extended stability range of phosphorus allotropes, Angew. Chem. Int. Ed. **53**, 11629 (2014).

[9] J. Guan, Z. Zhu, and D. Tománek, Phase Coexistence and Metal-Insulator Transition in Few-Layer Phosphorene: A Computational Study, Phys. Rev. Lett. **113**, 046804 (2014).

[10] Z. Zhuo, X. Wu, and J. Yang, Two-dimensional phosphorus porous polymorphs with tunable band gaps, J. Am. Chem. Soc. **138**, 7091 (2016).

[11] M. Ruck, D. Hoppe, B. Wahl, P. Simon, Y. Wang, and G. Seifert, Fibrous red phosphorus, Angew. Chem. Int. Ed. **44**, 7616 (2005).

[12] W. Hittorf, Zur kenntniss des phosphors, Ann. Phys. Chem. **202**, 193 (1865).

[13] H. Thurn and H. Krebs, Über struktur und eigenschaften der halbmetalle. XXII. Die kristallstruktur des hittorfschen phosphors, Acta Cryst. B **25**, 125 (1969).

[14] J. Zhou, T. Y. Cai, and S. Ju, Anisotropic exciton excitations and optical properties of Hittorf's phosphorene, Phys. Rev. Research **2**, 033288 (2020).

[15] J. C. Jamieson, Crystal structures adopted by black phosphorus at high pressures, Science **139**, 1291 (1963).

[16] D. Scelta, A. Baldassarre, M. Serrano-Ruiz, K. Dziubek, A. B. Cairns, M. Peruzzini, R. Bini, and M. Ceppatelli, Interlayer bond formation in black phosphorus at high pressure, Angew. Chem. Int. Ed. **56**, 14135 (2017).

[17] X. Li, J. Sun, P. Shahi, M. Gao, A. H. MacDonald, Y. Uwatoko, T. Xiang, J. B. Goodenough, J. Cheng, and J. Zhou, Pressure-induced phase transitions and superconductivity in a black phosphorus single crystal, Proc. Natl. Acad. Sci. USA **115**, 9935 (2018).

[18] A. Kundu, D. Tristant, N. Sheremetyeva, A. Yoshimura, A. T. Dias, K. S. Hazra, V. Meunier, and P. Puech, Reversible pressure-induced partial phase transition in few-layer black phosphorus, Nano Lett. **20**, 5929 (2020).

[19] Z. Zhu and D. Tománek, Semiconducting Layered Blue Phosphorus: A Computational Study, Phys. Rev. Lett. **112**, 176802 (2014).

[20] J. L. Zhang, C. Han, Z. Hu, L. Wang, L. Liu, A. T. S. Wee, and W. Chen, 2D phosphorene: Epitaxial growth and interface engineering for electronic devices, Adv. Mater. **30**, 1802207 (2018).

[21] J. L. Zhang, S. Zhao, C. Han, Z. Wang, S. Zhong, S. Sun, R. Guo, X. Zhou, C. D. Gu, K. D. Yuan, Z. Li, and W. Chen, Epitaxial growth of single layer blue phosphorus: A new phase of two-dimensional phosphorus, Nano Lett. **16**, 4903 (2016).

[22] C. Gu, S. Zhao, J. L. Zhang, S. Sun, K. Yuan, Z. Hu, C. Han, Z. Ma, L. Wang, F. Huo, W. Huang, Z. Li, and W. Chen, Growth of quasi-free-standing single-layer blue phosphorus on tellurium monolayer functionalized Au (111), ACS Nano **11**, 4943 (2017).

[23] J. P. Xu, J. Q. Zhang, H. Tian, H. Xu, W. Ho, and M. Xie, One-dimensional phosphorus chain and two-dimensional blue phosphorene grown on Au (111) by molecular-beam epitaxy, Phys. Rev. Mater. **1**, 061002(R) (2017).

[24] E. Golias, M. Krivenkov, A. Varykhalov, J. Sánchez-Barriga, and O. Rader, Band renormalization of blue phosphorus on Au (111), Nano Lett. **18**, 6672 (2018).

[25] J. Zhuang, C. Liu, Q. Gao, Y. Liu, H. Feng, X. Xu, J. Wang, J. Zhao, S. X. Dou, Z. Hu, and Y. Du, Band gap modulated by electronic superlattice in blue phosphorene, ACS Nano **12**, 5059 (2018).

[26] J. L. Zhang, S. Zhao, M. Telychko, S. Sun, X. Lian, J. Su, A. Tadich, D. Qi, J. Zhuang, Y. Zheng, Z. Ma, C. Gu, Z. Hu, Y. Du, J. Lu, Z. Li, and W. Chen, Reversible oxidation of blue phosphorus monolayer on Au (111), Nano Lett. **19**, 5340 (2019).

[27] J. L. Zhang, S. Zhao, S. Sun, H. Ding, J. Hu, Y. Li, Q. Xu, X. Yu, M. Telychko, J. Su, C. Gu, Y. Zheng, X. Lian, Z. Ma, R. Guo, J. Lu, Z. Sun, J. Zhu, Z. Li, and W. Chen, Synthesis of monolayer blue phosphorus enabled by silicon intercalation, ACS Nano **14**, 3687 (2020).

[28] D. Zhou, Q. Meng, N. Si, X. Zhou, S. Zhai, Q. Tang, Q. Ji, M. Zhou, T. Niu, and H. Fuchs, Epitaxial growth of flat, metallic monolayer phosphorene on metal oxide, ACS Nano **14**, 2385 (2020).

[29] J. Zeng, P. Cui, and Z. Zhang, Half Layer by Half Layer Growth of a Blue Phosphorene Monolayer on a GaN(001) Substrate, Phys. Rev. Lett. **118**, 046101 (2017).

[30] C. E. P. Villegas, A. S. Rodin, A. Carvalho, and A. R. Rocha, Two-dimensional exciton properties in monolayer semiconducting phosphorus allotropes, Phys. Chem. Chem. Phys. **18**, 27829 (2016).

[31] F. Iyikanat, E. Torun, R. T. Senger, and H. Sahin, Stacking-dependent excitonic properties of bilayer blue phosphorene, Phys. Rev. B **100**, 125423 (2019).

[32] M. R. Fiorentin, G. Cicero, and M. Palummo, Spatially indirect excitons in black and blue phosphorene double layers, Phys. Rev. Mater. **4**, 074009 (2020).

[33] J. Zhou, T. Y. Cai, and S. Ju, Unusual Strain Dependence of Quasiparticle Electronic Structure, Exciton, and Optical Properties in Blue Phosphorene, Phys. Rev. Appl. **15**, 024045 (2021).

[34] L. V. Keldysh, Coulomb interaction in thin semiconductor and semimetal films, JETP Lett. **29**, 658 (1979).

[35] L. Yang, J. Deslippe, C. H. Park, M. L. Cohen, and S. G. Louie, Excitonic Effects on the Optical Response of Graphene and Bilayer Graphene, Phys. Rev. Lett. **103**, 186802 (2009).

[36] P. Cudazzo, I. V. Tokatly, and A. Rubio, Dielectric screening in two-dimensional insulators: Implications for excitonic and impurity states in graphene, Phys. Rev. B **84**, 085406 (2011).

[37] D. Y. Qiu, F. H. da Jornada, and S. G. Louie, Optical Spectrum of MoS_2: Many-Body Effects and Diversity of Exciton States, Phys. Rev. Lett. **111**, 216805 (2013); **115**, 119901 (2015).

[38] T. C. Berkelbach, M. S. Hybertsen, and D. R. Reichman, Theory of neutral and charged excitons in monolayer transition metal dichalcogenides, Phys. Rev. B **88**, 045318 (2013).

[39] A. S. Rodin, A. Carvalho, and A. H. Castro Neto, Excitons in anisotropic two-dimensional semiconducting crystals, Phys. Rev. B **90**, 075429 (2014).

[40] S. Latini, T. Olsen, and K. S. Thygesen, Excitons in van der Waals heterostructures: The important role of dielectric screening, Phys. Rev. B **92**, 245123 (2015).

[41] D. Y. Qiu, F. H. da Jornada, and S. G. Louie, Screening and many-body effects in two-dimensional crystals: Monolayer MoS_2, Phys. Rev. B **93**, 235435 (2016).

[42] M. H. Naik and M. Jain, Origin of layer dependence in band structures of two-dimensional materials, Phys. Rev. B **95**, 165125 (2017).

[43] V. Tran, R. Soklaski, Y. Liang, and L. Yang, Layer-controlled band gap and anisotropic excitons in few-layer black phosphorus, Phys. Rev. B **89**, 235319 (2014).

[44] V. Tran, R. Fei, and L. Yang, Quasiparticle energies, excitons, and optical spectra of few-layer black phosphorus, 2D Mater. **2**, 044014 (2015).

[45] D. Y. Qiu, F. H. da Jornada, and S. G. Louie, Environmental screening effects in 2D materials: renormalization of the bandgap, electronic structure, and optical spectra of few-layer black phosphorus, Nano Lett. **17**, 4706 (2017).

[46] Y. Chen and S. Y. Quek, Tunable bright interlayer excitons in few-layer black phosphorus based van der Waals heterostructures, 2D Mater. **5**, 045031 (2018).

[47] Y.-H. Chan, D. Y. Qiu, F. H. da Jornada, and S. G. Louie, Giant exciton-enhanced shift currents and direct current conduction with subbandgap photo excitations produced by many-electron interactions, Proc. Natl. Acad. Sci. USA **118**, e1906938118 (2021).

[48] G. Onida, L. Reining, and A. Rubio, Electronic excitations: Density-functional versus many-body Green's function approaches, Rev. Mod. Phys. **74**, 601 (2002).

[49] P. Giannozzi, S. Baroni, N. Bonini, M. Calandra, R. Car, C. Cavazzoni, D. Ceresoli, G. L. Chiarotti, M. Cococcioni, I. Dabo, A. D. Corso, S. de Gironcoli, S. Fabris, G. Fratesi, R. Gebauer, U. Gerstmann, C. Gougoussis, A. Kokalj, M. Lazzeri, L. Martin-Samos *et al.*, QUANTUM ESPRESSO: A modular and open-source software project for quantum simulations of materials, J. Phys.: Condens. Matter **21**, 395502 (2009).

[50] J. P. Perdew, K. Burke, and M. Ernzerhof, Generalized Gradient Approximation Made Simple, Phys. Rev. Lett. **77**, 3865 (1996).

[51] D. R. Hamann, Optimized norm-conserving Vanderbilt pseudopotentials, Phys. Rev. B **88**, 085117 (2013).

[52] S. Grimme, Semiempirical GGA-type density functional constructed with a long-range dispersion correction, J. Comput. Chem. **27**, 1787 (2006).

[53] M. S. Hybertsen and S. G. Louie, Electron correlation in semiconductors and insulators: Band gaps and quasiparticle energies, Phys. Rev. B **34**, 5390 (1986).

[54] M. Rohlfing and S. G. Louie, Electron-hole excitations and optical spectra from first principles, Phys. Rev. B **62**, 4927 (2000).

[55] J. Deslippe, G. Samzonidze, D. A. Strubbe, M. Jain, M. L. Cohen, and S. G. Louie, BerkeleyGW: A massively parallel computer package for the calculation of the quasiparticle and optical properties of materials and nanostructures, Comput. Phys. Commun. **183**, 1269 (2012).

[56] B. C. Shih, Y. Xue, P. Zhang, M. L. Cohen, and S. G. Louie, Quasiparticle Band Gap of ZnO: High Accuracy from the Conventional G^0W^0 Approach, Phys. Rev. Lett. **105**, 146401 (2010).

[57] C. D. Spataru, S. Ismail-Beigi, R. B. Capaz, and S. G. Louie, Theory and *Ab initio* Calculation of Radiative Lifetime of Excitons in Semiconducting Carbon Nanotubes, Phys. Rev. Lett. **95**, 247402 (2005).

[58] M. Palummo, M. Bernardi, and J. C. Grossman, Exciton radiative lifetimes in two-dimensional transition metal dichalcogenides, Nano Lett. **15**, 2794 (2015).

[59] J. Ahn, I. Hong, Y. Kwon, R. C. Clay, L. Shulenburger, H. Shin, and A. Benali, Phase stability and interlayer interaction of blue phosphorene, Phys. Rev. B **98**, 085429 (2018).

[60] M. R. K. Musa, C. Zhang, M. Rajapakse, J. B. Jasinski, G. Sumanasekera, and M. Yu, Li interaction-induced phase transition from black to blue phosphorene, Phys. Rev. Mater. **5**, 024007 (2021).

[61] J. Arcudia, R. Kempt, M. E. Cifuentes-Quintal, T. Heine, and G. Merino, Blue Phosphorene Bilayer is a Two-Dimensional Metal and an Unambiguous Classification Scheme for Buckled Hexagonal Bilayers, Phys. Rev. Lett. **125**, 196401 (2020).

[62] A. Marini, *Ab Initio* Finite-Temperature Excitons, Phys. Rev. Lett. **101**, 106405 (2008).

[63] J. Noffsinger, E. Kioupakis, C. G. Van de Walle, S. G. Louie, and M. L. Cohen, Phonon-Assisted Optical Absorption in Silicon from First Principles, Phys. Rev. Lett. **108**, 167402 (2012).

[64] J. Choi, P. Cui, H. Lan, and Z. Zhang, Linear Scaling of the Exciton Binding Energy Versus the Band Gap of Two-Dimensional Materials, Phys. Rev. Lett. **115**, 066403 (2015).

[65] T. Olsen, S. Latini, F. Rasmussen, and K. S. Thygesen, Simple Screened Hydrogen Model of Excitons in Two-Dimensional Materials, Phys. Rev. Lett. **116**, 056401 (2016).

[66] Z. Jiang, Z. Liu, Y. Li, and W. Duan, Scaling Universality between Band Gap and Exciton Binding Energy of Two-Dimensional Semiconductors, Phys. Rev. Lett. **118**, 266401 (2017).

[67] M. L. Cohen and S. G. Louie, *Fundamentals of Condensed Matter Physics* (Cambridge University Press, Cambridge, UK, 2016).

[68] L. D. Whalley, J. M. Frost, B. J. Morgan, and A. Walsh, Impact of nonparabolic electronic band structure on the optical and transport properties of photovoltaic materials, Phys. Rev. B **99**, 085207 (2019).